Study of the Casting of Sulfonated Polyimide Ionomer Membranes: Structural Evolution and Influence on Transport Properties

ARTICLE *in* THE JOURNAL OF PHYSICAL CHEMISTRY B · JULY 2005

Impact Factor: 3.3 · DOI: 10.1021/jp0500586 · Source: PubMed

5 AUTHORS, INCLUDING:

Anne-Laure Rollet
CNRS
54 PUBLICATIONS **1,021** CITATIONS
SEE PROFILE

Olivier Diat
Atomic Energy and Alternative Energies Com…
148 PUBLICATIONS **4,296** CITATIONS
SEE PROFILE

Study of the Casting of Sulfonated Polyimide Ionomer Membranes: Structural Evolution and Influence on Transport Properties

Anca-Nicoleta Galatanu,[†] Anne-Laure Rollet,*[,‡] Patrice Porion,[§] Olivier Diat,[†] and Gérard Gebel[†]

Structures et Propriétés des Architectures Moleculaires, UMR SPrAM 5819, DRFMC/SPrAM, CEA-CNRS-UJF, CEA-Grenoble, 38054 Grenoble Cedex 9, France, CNRS/Centre de Recherche sur les Matériaux à Haute Température, 1D av. de la Recherche Scientifique, 45071 Orléans Cedex 2, France, and CNRS/Centre de Recherche sur la Matière Divisée, 1 bis, rue de la Férollerie, 45071 Orléans Cedex 2, France

Received: January 5, 2005

A casting process has been studied for charged polymers: the sulfonated polyimide ionomer membrane. The formation of the membrane has been followed by X-ray reflectivity as a function of temperature. The effect of equivalent weight has been also investigated. The thickness loss presents two regimes: the first one is linear vs time indicating that the models developed for noncharged polymer may be suitable for ionomers in the early period of drying. The second one corresponds to the loss of X-ray reflectivity signal. Moreover, the X-ray reflectivity signal seems to be correlated to the characteristic time of the sample drying. In complement, we have studied the influence of casting on the properties of the dried ionomer membranes. The transport coefficients of $N(CH_3)_4^+$ ions confined in two kinds of membranes that were differently cast were measured. The results show that shearing the ionomer solution during casting may lead to an enhancement of the anisotropy of structure and of transport. Moreover, we have studied the effect of both interfaces on the ion transport properties through the dried membranes.

1. Introduction

The numerous works and publications reflect the great interest in proton exchange membrane fuel cell (PEMFC). All the aspects of this technology are treated: nature of ionomer membranes, gas permeation, electrodes, fuel storage, etc. With concern to the membrane itself, most of the studies deal with the perfluorosulfonated Nafion due to its properties:[1] chemical inertia to acid media, long life spent, good ionic conductivity, superselectivity. The Nafion perfluorosulfonated polymer chains organization is not completely understood yet. However, recent works propose a structure consisting in long cylinders of polymer chains (length > 1000 Å, radius = 40 Å) covered by the anionic sulfonate groups.[2,3] These cylinders do not seem to have a particular organization, and the structure of Nafion appears to be quasi-isotrope at large scale. The electrolyte solutions locate inside the network of these cylinders and determine an isotropic important swelling of the membrane size (about 30%). Moreover, one has to keep in mind that the Nafion properties depend on the external conditions (nature and concentration of electrolyte, temperature, etc.).[4] Despite the good properties of Nafion ionomer membrane, its high cost has determined several research groups to develop new ionomer membranes as an alternative such as sulfonated poly ether ether ketone,[5] sulfonated polysulfone,[6] and sulfonated polyimide (sPI). From the several kinds of the sPI ionomers developed by different research groups,[7−9] we are interested in the naphthalenic ones.

This kind of block copolymer exhibits interesting properties for fuel cell applications: high ionic selectivity, high conductivity,[10,11] interesting gas permeation properties,[12] small geometrical variations during swelling−deswelling cycles due to a high vitreous transition temperature (Tg about 270 °C). Most of its physicochemical properties are rather different from Nafion's. The first point is the rigidity of the polymer chains induced by the aromatic cycles. Structural anisotropy has been detected at the nanometer scale by small-angle X-ray and neutrons scattering (SAXS and SANS, respectively) and at the micrometer scale by optical microscopy[13] and ionic transport properties.[14] The structural anisotropy leads also to an anisotropic swelling: the latter occurs only along the thickness. The second point is that the charges are carried by the main chain in contrast to Nafion where sulfonate groups are located on pendent chains. This leads to a lower segregation between hydrophobic and hydrophilic domains. The third important point is that the structural properties are not sensitive to the external conditions (nature and concentration of electrolyte, temperature) as it is the case for Nafion.[4] These observations induce many questions on the process of membrane formation from ionomer solutions and their consequences on the properties. Several studies have already been devoted to the influence of casting on the structure of noncharged polymer membranes. This research has lead to new processes[15] such as vapor-induced phase separation (VIPS),[16,17] where the casting solution is dried under an atmosphere containing nonsolvent vapor, i.e., the vapor of an another solvent than the one used in the polymer solution and that is poor solvent of the polymer. To our knowledge, there is no study devoted to the influence of casting on charged polymer membranes, i.e., ionomer membranes. The charges by inducing a preoganization of polymer chains in the initial solution are expected to greatly modify the behavior toward casting. This work is a first step to understand the influence of casting on

* To whom correspondence may be addressed. E-mail: rollet@cnrs-orleans.fr.
[†] Structures et Propriétés des Architectures Moleculaires.
[‡] CNRS/Centre de Recherche sur les Matériaux à Haute Température.
[§] CNRS/Centre de Recherche sur la Matière Divisée.

10.1021/jp0500586 CCC: $30.25
Published on Web 05/14/2005

sPI ionomer membranes. Here, the drying conditions were the simplest, that is, ionomer solutions were drying under an ionomer solvent (*m*-cresol) atmosphere without any other solvent. This paper is an attempt to correlate the transport properties of complete membranes that were differently cast and the structural evolution during drying. In the first section, we studied the difference of ion diffusion inside membranes that had or had not undergone shearing process during drying. In addition, we investigated the effect of the membrane surface. We measured the ion diffusion through two kinds of sPI surfaces. One was in contact with glass medium during drying and another was in contact with air. In the second section, we attempt to throw light on the transport results by studying the drying process by X-ray reflectivity.

2. Experimental Section

2.1. Ionomer. The chemical fomula of sulfonated naphthalenic polyimide ionomer is given below.

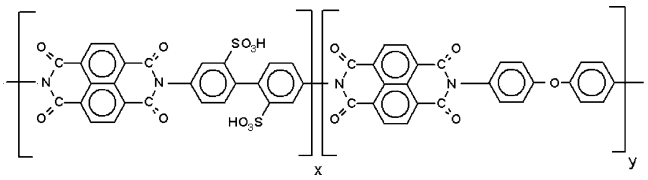

X is the mean number of sulfonated monomers and Y the mean number of hydrophobic blocks in the polymer sequence. The number of charges in the polymer chains is defined through the mass of polymer carrying 1 mol of charges (SO_3^-), that is, through the equivalent weight noted EW in the following. In this study, the EW = 792 g/equiv with X = 5 and Y = 12. In the X-ray study part, a complement was made with EW = 504 g/equiv and X = Y = 5 sPI. Complementary information on these sPI ionomers can be found in previous papers.[7,8] The sPI ionomer is in a *m*-cresol solution.

2.2. Ionomer Solution Drying. *2.2.1. Transport Study.* We compare the properties of sPI membranes prepared by the standard method, noted (1), and by a slower and less stressful one, noted (2). (1) In the "industrial" protocol, the solution of sPI in *m*-cresol was heated at 110 °C and filtered. Then, the solution is cast using hand coating, i.e., it was spread out over a hot plate made in Pyrex using a kind of ruler. The drying was performed under a laminar flux of air in order to prevent dust from deposing on the membrane surface. The heating cycles were the following: 2 h at 50 °C, 16 h at 65 °C, and finally 4 h at 75 °C. The goal of these cycles is to prevent as much as possible the formation of a crust on the membrane surface. The final thickness of the sample is constant all over the membrane and is about 63 μm. (2) In the slower and less stressful protocol, the ionomer solution was simply poured over Pyrex pot placed on a hot plate. The spreading was done only by gravity and in a limited area (8 × 15 cm). We were thus obliged to put an important quantity of polymer solution in order to obtain a regular enough membrane thickness. The final sample thickness was about 220 μm. Because of the great quantity of spread ionomer solution, we were obliged to use a softer drying temperature than set (1), otherwise the dried sample would not have a film shape. The drying consisted in only one heating cycle at 40 °C, and a funnel was placed over the drying membrane in order to control the solvent evaporation rate. The operation lasted here 15 days.

Once dried, the membranes were released from the support by immersion in water. Then, they were placed in reflux in boiling methanol in order to remove the *m*-cresol left. Finally, they were acidified by immersion in a 0.1 M HCl solution.

The membranes were then neutralized by $N(CH_3)_4^+$ or Na^+ ions by immersion in highly concentrated solutions of $N(CH_3)_4$-Cl or NaCl, and after a sufficient time they were rinsed several times with pure water. For the NMR experiments, we used heavy water to prevent signal saturation by H_2O. For the radiotracer experiments, we could not perform in pure water as one followed the exchange of radiolabeled species contained in the membrane with nonradiolabeled species contained in the external solution (see experimental description). In the latter case, the external solution concentration was 10^{-1} mol/L.

2.2.2. X-ray Reflectivity Study. During the experiments, the sample was placed into an aluminum rectangular cell (0.2 × 0.08 × 0.5 m^3) with Kapton windows allowing the X-rays to pass through. The cell was kept closed and was connected to a water bath that controlled the temperature with a precision of 0.01 °C. The given temperature is the one inside of the cell and was measured by a contact probe. Experiments were carried out in a reflectivity-like configuration, during the process of drying. Samples of different polymer concentrations were measured at several temperatures. The incident and reflected angles were kept fixed, and the intensity of X-rays was measured during intervals of 10 min, after which the sample position into the beam was readjusted.

The initial concentration of ionomer solution in *m*-cresol solvent was 8 wt %. Samples of different concentrations were investigated during the process of drying, at several temperatures and incident angles of X-rays. Thick polymer solution (2000 μm) were cast from *m*-cresol solvent onto a glass plate. After drying were obtained membranes of 80- to 100-μm controlled thickness. They could be unstuck from the glass lamella support by peeling them off.

2.3. Conductivity. The conductivity experiments have been carried out with a mercury cell,[18] as previously described.[19] A piece of swollen membrane separates 2 compartments filled with Hg; the surface in contact with these electrodes is 0.383 cm^2. The conductivity is thus measured in the transverse direction. A Paar 273 as potentiostat and a Solartron SI1255 as frequency analyzer were used for impedance measurements. The spectra were recorded over a frequency ranging from a few Hz to several hundred kHz. The value of the membrane resistance was determined when the imaginary part of the impedance is equal to zero (frequency about 50 kHz).

2.4. Radiotracers. The radiotracer method used in the present work to determine the $N(CH_3)_4^+$ self-diffusion coefficients in sPI membranes is based on the rotating-electrode principle. A circular piece of membrane of 1 cm in diameter was glued on a Plexiglas cylinder with mastic. The cell was first immersed into an electrolyte solution of a given molality *m* (0.1 mol/kg). When equilibrium was reached, it was introduced into a radiolabeled ($^{14}CH_3N(CH_3)_3^+$) electrolyte solution of the same composition. At equilibrium, the cell was mounted on a rotating electrode spindle and immersed into a nonradioactive solution of molality *m*. Then successive aliquots of this solution were taken as a function of time. The aliquot radioactivity is measured, and the transverse self-diffusion coefficient *D* is obtained by fitting the ratio of inner over outer radioactivity as a function of time. It is important to notice that with such experimental device only one interface of the membrane is crossed by the radiotracers. We can thus study selectively the influence of each interface on the transport of ions through the membrane. The whole system was thermostated at 298 K during the experiment. This experimental setting allows us to measure

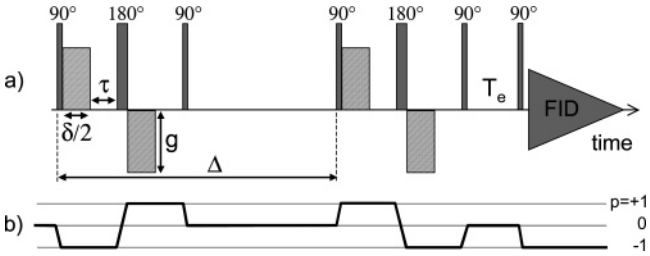

Figure 1. (a) Schematic view of the BPP LED PFG sequence (see text). (b) Coherence-transfer pathway ($p = 0 \rightarrow -1 \rightarrow +2 \rightarrow -1 \rightarrow +1 \rightarrow -2 \rightarrow +1 \rightarrow -1$) resulting from an adequate phase cycling.

TABLE 1: Values of Conductivity of SPI and Nafion Membranes Neutralized by $N(CH_3)_4^+$ or Na^+ Ions

ionomer membrane	counterions	χ (S/cm)
sPI, set 2	$N(CH_3)_4^+$	2.17×10^{-3}
sPI, set 1	$N(CH_3)_4^+$	0.22×10^{-3}
Nafion 115	$N(CH_3)_4^+$	0.73×10^{-3}
sPI, set 2	Na^+	4.65×10^{-3}
sPI, set 1	Na^+	1.39×10^{-3}
Nafion 115	Na^+	6.31×10^{-3}

transverse self-diffusion coefficient. More details on this experimental setup are given in a previous publication.[20]

The experiments have been repeated five times, and the values reported in Table 1 are the averages. The radiolabeled $^{14}CH_3N(CH_3)_3^+$ species are β emitters; the aliquots (50 μL) were then mixed with 5 mL of Aqualyte JT Baker scintiller liquid. The radioactivity was counted by Packard Tri-Carb 2100CR.

2.5. NMR. The self-diffusion coefficient of $N(CH_3)_4^+$ ions have been measured by pulsed-field gradient spin−echo (PFGSE) NMR. In this study, we have used a BPP LED PFG sequence (bipolar pulse pairs longitudinal eddy current delay pulsed field gradient) developed by Wu et al.[21] from the well-known 13-interval bipolar gradient pulses sequence of Cotts et al.[22] The NMR sequence is represented in Figure 1. This sequence allows the suppression of the distortion of the diffusion results due to the internal magnetic field gradients, which can be induced by the susceptibility variations present in heterogeneous samples. In PFGSE measurements, the spins are labeled at time $t = 0$ with respect to their position in a given direction by applying a pulse of magnetic field gradient along this direction; after an evolution time called diffusion time Δ, a second pulse of magnetic field gradient opposite to the first one is applied. This second pulse cancels the effect of the first one, unless the spins have moved during the time Δ. If the spins have diffused, the second gradient pulse does not refocus all the spins and the echo signal is less intense. This decrease is a function of the self-diffusion coefficient D. In these experiments, a 4×4 cm^2 piece of membrane was rolled and put in an NMR tube of 4 mm in diameter. In such a configuration, the membrane surface is collinear to the static magnetic field $\mathbf{B_0}$ and the self-diffusion coefficient (noted D_{Pr}) was only determined in the direction parallel to the membrane surface since the gradient pulse was only applied along the direction collinear to $\mathbf{B_0}$. The echo attenuation $S(q)$ measured using this sequence is

$$S(q) = S(0) \exp[-4\pi^2 D q^2 (\Delta - \delta/3 - \tau/2)]$$

where $q = \gamma g \delta / 2\pi$, γ is the gyromagnetic ratio of proton, g is the magnetic gradient field strength, and δ is the gradient pulse width. The time Δ is the diffusion time, i.e., the time during which the ions diffuse, and τ is a short delay to avoid the distortion of the echo by the eddy currents caused by the gradient switching (typically few hundred microseconds). An additional longitudinal eddy current delay T_e is also used to reduce eddy current distortions (few ms). This sequence is repeated with 16 rising gradient strengths g and D_{Pr} is obtained by a fit of $\ln(S(q)/S(0))$ vs q^2. In this study, Δ ranged from 5 to 1000 ms, the gradient strength g from 0 to 1.6 T/m with a gradient pulse width δ varying between 1 and 5 ms. The measurements have been performed using a DSX100 Bruker spectrometer and a magnetic resonance imaging probehead (Micro5 Bruker). For all the NMR experiments, the solvent was D_2O and not H_2O as for the other transport measurements performed in this paper. Moreover, the NMR measurements have been performed for ionomer without added salt.

2.6. X-ray Reflectivity. The X-ray experiments with synchrotron radiation were performed at beamline ID10B at the ESRF, Grenoble, France. This beamline is constructed as a six-circle goniometer, with possibility of a reflectivity configuration. The apparatus consisted of a collimation system, a sample goniometer system, and a detector system. The incident X-ray beam is monochromized by a double-crystal monochromator consisting of a pair of parallel Si(111) crystals. The wavelength of incident beam was adjusted to be 1.54 Å by this monochromator. Incident X-rays passed through a He guide tube; after that, X-rays travelled in air. The intensity of the incident X-rays was monitored with two ion chambers. The beam was then collimated by several slits. A wheel with different thicknesses of Al plates situated in front of the sample was used as an attenuator to protect the scintillation counter from radiation damage by the strong direct beam or totally reflected beam.

The sample goniometer system consisted of a goniometer and a sample stage. Measurements were performed so that the scattering angle 2θ was a double portion of the incident angle θ; in other words, the reflectivity was measured for the reflection angle being equal with the incident angle. This is known as a specular reflection. The typical angle used during the experiments was 0.35°. The sample stage could be moved vertically, permitting in this way to follow the evolution of the membrane thickness. Optical alignment was performed by moving the sample stage into the beam so that the intensity of the reflected beam was at half value of the totally reflected beam.

The reflected X-rays beam passed through a slit whose gap was the same as that for the incident X-rays. This slit was used to reduce the effect of diffuse scattering at the membrane surface. The intensity data of reflected X-rays was detected with a position-sensitive detector.

We investigated the drying behavior of sPI by X-ray reflectivity measurements. This method is generally used for measurement of thickness of thin polymer membranes (~300 nm). The thickness determination accuracy is very high; the estimated error is less than 1 nm.[28]

3. Results

3.1. Transport Properties. Two membrane sets cast in different manners have been studied: (1) by the standard protocol using hand coating and (2) by a simple pouring without shearing. All the results are listed in Tables 1 and 2.

(1) Such a shaping process is expected to induce important shearing of the polymer solution and thus to lead to a preferential orientation of the polymer chains in the membrane. Previous SAXS studies have indeed revealed a strong structural anisotropy at the nanometer scale in this kind of membrane.[13] In this work, the transport in the transverse direction to the membrane surface was first studied at small scale using conductivity measurements. The values are reported in Table 1. The conductivity χ of $N(CH_3)_4^+$ in this membrane is 2.2×10^{-4}

TABLE 2: Self-Diffusion Coefficients of $N(CH_3)_4^+$ Ions Confined in sPI Membranes Measured by Several Techniques

ionomer membrane	counterions	technique	D (m^2/s)
sPI, set 2	$N(CH_3)_4^+$	D_{PR}, NMR CEA	12×10^{-12}
sPI, set 2	$N(CH_3)_4^+$	D_{PR}, NMR CRMD	9.2×10^{-12}
sPI, set 2	$N(CH_3)_4^+$	D, radiotracer "glass" side	9.2×10^{-12}
sPI, set 2	$N(CH_3)_4^+$	D, radiotracer "air" side	7.2×10^{-12}
sPI, set 1	$N(CH_3)_4^+$	D, radiotracer	1.52×10^{-12}
sPI, set 2	$N(CH_3)_4^+$	D, conductivity	33.2×10^{-12}
sPI, set 1	$N(CH_3)_4^+$	D, conductivity	3.38×10^{-12}

Ω^{-1} cm^{-1}, which is 3.3 times lower than in the Nafion 115 membrane (7.3×10^{-4} Ω^{-1} cm^{-1}). Such a comparison has to be balanced by the ionic capacity of the membrane because this parameter strongly influences the conductivity.[23,11] It is of 1100 g/equiv for Nafion and 792 g/equiv for sPI. At equal ionic capacity, the sPI membrane conductivity would be much lower than the Nafion one. Several factors may be responsible for it. First, in contrast to Nafion, the sulfonate charges in sPI are carried by the main ionomer chain, and in consequence, the hydrophilic domains of sPI are obstructed by these chains. Second, there is the strong ordering of the polymer chains observed through the high anisotropy of the membranes.[13] It is difficult with the available data to find out which is the predominant factor. To compare the conductivity and the radiotracer measurements, one can derive the self-diffusion coefficient of $N(CH_3)_4^+$ from the conductivity using the Nernst−Einstein relation ($D_i = \chi_i RT/F^2C_i$): the obtained value is 3.4×10^{-12} m^2/s. Note that the characteristic time in our conductivity experiments is about 10^{-5} s, and it corresponds, by using the relation $L = (2D\Delta)^{1/2}$, to a distance about several nanometers. In radiotracer measurements, the characteristic time is much larger as it is about several tens of seconds. In this case, the self-diffusion coefficient of $N(CH_3)_4^+$ is equal to 1.5×10^{-12} m^2/s. A factor equal to 2.2 separates the two values of the self-diffusion coefficient. This may be attributed to the multi-scale organization of the polymer chains in the membrane, i.e., to the existence of structure which characteristic size is much greater than the characteristic length explored in conductivity experiments.

(2) For the second set of membranes, the polymer solution was simply poured. The shearing is much smaller. The conductivity of $N(CH_3)_4^+$ in this membrane is equal to 2.2×10^{-3} Ω^{-1} cm^{-1}, which is 10 times higher than the sample shaped by hand coating. The surprising point is that the conductivity of the second set of membranes is significantly higher than the Nafion one. Nevertheless, this difference being dependent on the counterions, we have also measured the conductivities of sPI and Nafion membranes neutralized by Na^+ ions. The values are reported in Table 1. With Na^+ ions, the order of conductivities follows the usual sequence: Nafion > sPI. The particular case of $N(CH_3)_4^+$ ions is very interesting because it may throw light on new aspects of the correlation between structure and interionic interactions. In the case of sPI membranes, we have observed the following facts: the smaller the EW, the smaller is the ratio of Na^+ conductivity on $N(CH_3)_4^+$ conductivity,[14] and the higher block length X, the smaller is the ratio. In terms of structure, the smaller the EW, the less ordered are the ionomer chains in the membranes. This latter point seems more closely related to our present observation: for the second set which is expected to be the less ordered sample, the ratio is only 2.1, whereas it is 6.3 for the first set. In all cases, the conductivity in the second set of membrane is much higher than in the first set. This can be attributed to the strong shearing occurring in the first samples set. As stated previously, we can compare the self-diffusion coefficient derived with the Nernst−Einstein relation, equal here to 33.2×10^{-12} m^2/s with the self-diffusion coefficient measured using radiotracers, equal to 9.2×10^{-12} m^2/s. For this set of membranes, the factor separating the two values is 3.2. This difference shows that the polymer structural organization at the micrometer scale is not induced by the shearing occurring during membrane casting but by the chemical properties of the polymer itself.

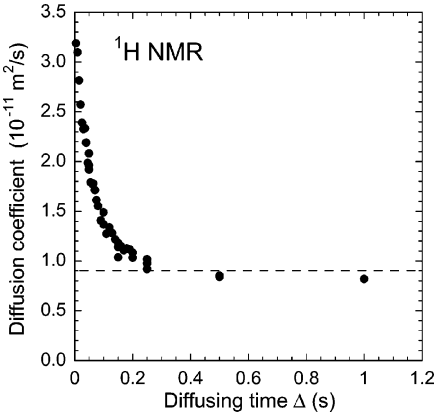

Figure 2. Self-diffusion coefficient D_{Pr} of the $N(CH_3)_4^+$ ions vs the observation time Δ in the direction parallel to the membrane plan (cast process 2).

As already mentioned, the anisotropy is expected to be much lower in the second set of sample. To verify this hypothesis, the self-diffusion coefficient of $N(CH_3)_4^+$ ions in the second set of membranes was measured in the direction parallel to the membrane plan. Unfortunately, the use of the radiotracers method is impossible in this case because the time needed for one experiment would last several months. For this reason, the supplementary measurements have been performed using PFGSE NMR. As it can be seen in Figure 2, the value of the diffusion coefficient D_{Pr} is a function of the diffusion time Δ (D_{Pr} decreases when Δ increases). This is a signature of restricted diffusion.[24−26] This phenomenon is characteristic of a diffusion process occurring in porous media and has been already observed in sPI membranes.[13] The term "porous" in this case is ambiguous because it does not refer to real pores but to domains where the transport properties are faster and that are connected to each other thus forming a network. The diffusion dependence on observation time Δ can be shortly explained as followed. At short time Δ, the ions do not have enough time to explore the structure and to encounter the walls of the "pore", and D is then equal to the one in nonconfined solution D_0; for a time large enough, the ions encounter the walls and as their pathway is restricted: $D(\Delta)$ is smaller than D_0. The bigger Δ, the smaller D, until Δ is sufficiently large so that ions have explored the whole representative volume of the sample. So, at long times, when the self-diffusion coefficient does not depend anymore on the observation time Δ (see the plateau in Figure 2), the effect of the structure is averaged. From this time, the ions diffuse in a volume larger than the representative volume of the porous medium.

From the time of the behavior change and its corresponding self-diffusion coefficient, the characteristic volume of the structure can be derived: for $\Delta = 0.4$ s and $D_{Pr} = 9 \times 10^{-12}$ m/s, $L = (2D\Delta)^{1/2} = 2.7$ μm. In previous NMR studies of sPI membranes (cast process 1),[14] the time of the behavior change was found to be larger (around 1 s) and the characteristic volume was about 4 μm. This shows that the heterogeneity of the sPI structure at the micrometer scale extends to a smaller distance when the ionomer solution is cast slowly without shearing phenomena. The plateau value can then be compared to the

value obtained with the radiotracer method: the two values are approximately equal. This confirms that the structure of the second set of the membrane is not as anisotropic as is the case in the first set. The comparison between these two sets of membranes shows the importance of the casting on the properties of the ionomer membrane. The hand-coating method induces a strong anisotropy of the membrane structure but not the existence of a structural organization at the micrometer scale. Moreover, this confirms that the structure anisotropy is the key point that explains the difference of conductivity between Nafion and sPI.

On the second set of membranes, we have also explored the effect of the interface during drying on the transport properties of the membrane. As described in the Experimental Section, the ionomer solution was spread onto a simple glass lamella and dried under air. In consequence, one face of the membrane was in contact with a "hydropholic" medium: glass with SiOH groups; moreover, this membrane interface does not undergo the evaporation phenomenon. The other face was in contact with a "hydrophobic" medium: air. Thanks to the radiotracer method used in this work, we can study the difference between these two faces in regard to diffusion. We have determined the self-diffusion of $N(CH_3)_4^+$ ions in the sPI membrane and crossing one or the other membrane face using the radiotracer method in two different configurations. (i) One piece of membrane was glued on the rotating spindle by the face that was in contact with air during the drying process, and let us note it "air". (ii) The other piece was glued by the other face, i.e., the one in contact with glass during drying, and let us note it "glass". Note that, for NMR and conductivity experiments, the transport coefficients are measured in the bulk of sample and no interface is crossed by ions.

The values (average over 5 experiments) obtained for each configuration are significantly different. The apparent self-diffusion coefficient with the "air" sample D_{air} is equal to $7.2 \times 10^{-12} \pm 0.2$ m^2/s, whereas the apparent self-diffusion coefficient with the "glass" sample D_{glass} is equal to $9.2 \times 10^{-12} \pm 0.2$ m^2/s. It points out that the two interfaces are different in the point of view of ion transport. The interface may be considered as a barrier to ions and solvent transport and it appears smaller in the case of the interface "air" than in the case of interface "glass". Because the drying time is long, the ionomer chains seem to be able to organize by minimizing the interface energy and the interaction between ionomer chains. In such dynamical phenomenon, the time of drying as well as the viscosity of the polymer solution are expected to be important parameters that control the properties of the membrane interface.

3.2. X-ray Synchrotron Reflectivity. In this section, we study the drying process of solutions of sulfonated polyimides in *m*-cresol.

In a first step, we have recorded the X-ray reflectivity spectra for several thicknesses at time $t = 0$ in order to guarantee us that the initial thickness did not affect the study. The results were independent of the initial thickness. Moreover, the nondependence on thickness is characteristic of the early period in the drying process of noncharged polymer solutions, the so-called "constant-rate period" (CRP).[27] During this early period of drying, the moisture concentration at the interface is constant and enough solvent remains in the bulk sample to migrate toward the interface. It can be noticed that, for porous materials, the CRP occurs over a large range of moisture concentration in the sample (up to 30%). In this regime, the external conditions (vapor pressure, etc.) rule the drying process.

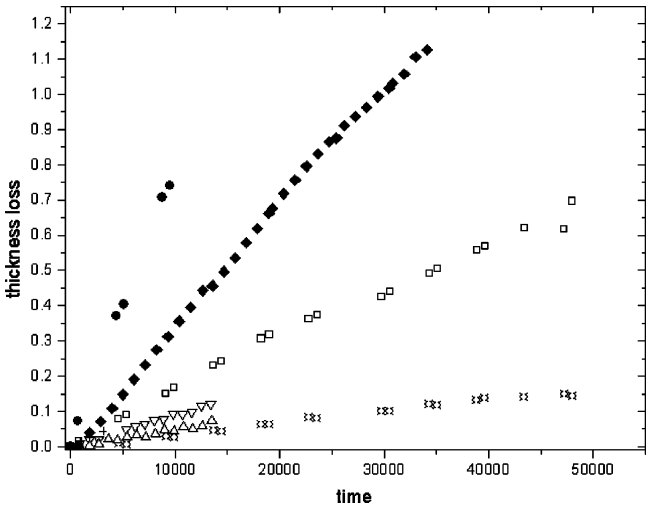

Figure 3. Variation of the thickness loss vs time of sPI (EW = 792 g/equiv and X = 5) ionomer solution of 8 wt % for several temperatures: (open circle) 20 °C, (up triangle) 42.3 °C, (down triangle) 50.9 °C, (cross) 53.2 °C, (open square) 58 °C. The result for a sPI (EW = 504 g/equiv and X = 5) ionomer solution at 55 °C has been also plotted (black diamond). For comparison, the water is represented with the gray circle.

The first information from X-ray measurements concerns the loss of the membrane thickness during the process of drying which is directly connected with the kinetic of drying. The thickness was determined at $\theta = 0°$ by measuring the intensity as a function of the sample position in the X-ray beam. The variation of the thickness as a function of time is presented in Figure 3. For the sPI X = 5 and EW = 792 g/equiv, the effect of temperature has been investigated. The higher the temperature, the faster is the kinetics of drying. The dependence of thickness loss is linear for long. As it can be seen in Figure 4a, the slope dependence on temperature is strongly nonlinear. One thus has to pay great attention on the temperature during membrane drying. We must complement this point with the following macroscopic observations: the dried membrane can take very bizarre shapes, such as fried egg, for a high drying temperature. Moreover, if one removes the drying membrane from the hot plate, the drying is stopped because of the low vapor pressure of *m*-cresol. The variation of the thickness loss slope (let us note it STL) is plotted vs the vapor pressure of *m*-cresol in Figure 4b. The values of vapor pressure have been derived using the Clausius−Clapeyron relation. We see in Figure 4b that STL is linearly dependent on the vapor pressure. Thus, as for noncharged polymer during CRP, the drying is controlled by the external parameters. In consequence, the models developed to describe the drying of noncharged polymers during this early period of drying may be suitable for ionomers. The reflectivity signal can be recorded until the surface roughness becomes high. The corresponding time depends on the sample characteristics, but it lasts several hours. During this period, the thickness loss describes a monotonic curve, quasilinear. It seems that we are in CRP until the degradation of the surface quality. An emerging question is: is the degradation of the surface the signature of the end of CRP? To determine if we are or if we are not in a CRP regime, the drying membranes were weighted in the course of time. The results are plotted in Figure 5a. At 52 °C, the weight loss $m(t)/m(t = 0)$ decreases linearly until 350 min approximately, and then the decrease slows down. We have also reported the time limits where the

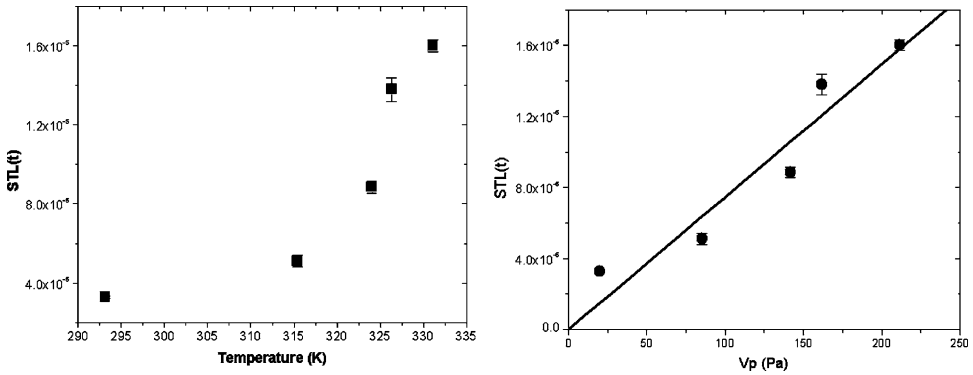

Figure 4. (a) Variation of the slope thickness loss in the course of time of sPI (EW = 792 g/equiv and X = 5) ionomer solution of 8 wt % as a function of the temperature. (b) Variation of the slope thickness loss with time of sPI (EW = 792 g/ equiv and X = 5) ionomer solution of 8 wt % as a function of the vapor pressure of *m*-cresol.

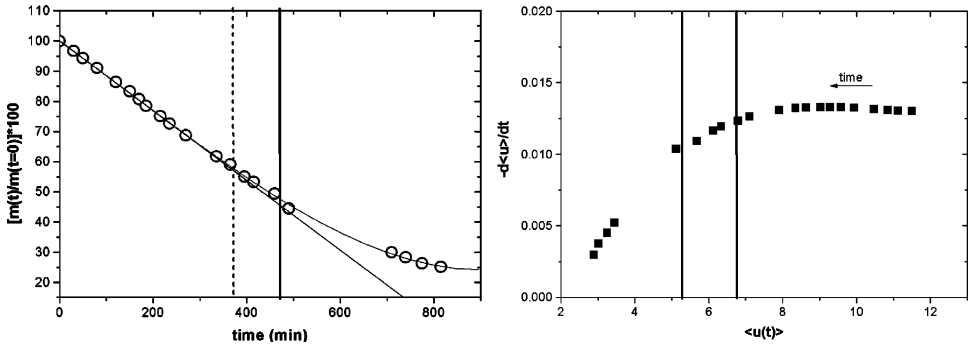

Figure 5. Variation of the weight loss vs time of sPI (EW = 792 g/equiv and X = 5) ionomer solution of 8 wt % at 52 °C and variation of $-d\langle u\rangle/dt$ vs $\langle u\rangle$. A line is plotted to help the reader to see when the decrease is not linear anymore. The dashed line represents the beginning of the degradation of the X-ray signal, and the full line represents the limit when reflectivity signal cannot be measured anymore.

reflectivity signal begins to be degraded and where it cannot be measured anymore. It seems that the surface degradation begins shortly after the end of the linear regime of weight loss. The usual way of representing the drying kinetic is to plot $-d\langle u\rangle/dt$ vs $\langle u\rangle$, where $\langle u\rangle$ is the mean solvent concentration. The characteristic figure is a plateau for high value of $\langle u\rangle$, which corresponds to CRP, and for small $\langle u\rangle$, i.e., a long drying time, $-d\langle u\rangle/dt$ increases with $\langle u\rangle$. Since the ionomer concentration is low, one can assume that the *m*-cresol concentration and weight loss are linearly dependent and calculate $-d\langle u\rangle/dt$ and $\langle u\rangle$. The results are plotted in Figure 5b with the same time limits as in Figure 5a. Shortly after the plateau, corresponding to the CRP, the reflectivity peak begins to broaden dramatically and it is finally lost 2 h later or 10% of supplementary weight loss. It seems that there is a correlation between the end of CRP and the degradation of the surface as seen by X-ray reflectivity measurements.

The typical X-ray reflectivity spectra recorded with our samples are presented in Figure 6. Note that the thickness of the membrane is very high (2000 μm) compared with the usual sample thickness used in X-ray reflectivity measurements (0.3 μm). The results and analysis are thus quite different. The peaks change slowly in the course of time: a slight decrease of the intensity along with a slight increase of half width at half maximum (HWHM) is observed, and quite abruptly, the reflectivity signal is lost.

The normalized reflected intensity is presented in Figure 7 for two temperatures: 42.3 and 50.9 °C. The measurement on the 42.3 °C sample has been stopped at the loss of reflectivity signal. In both cases, the decrease of the intensity is very slow: 2% per hour at 42.3 °C and 3% at 50.9 °C. The X-ray reflectivity intensity is correlated with the quality of the surface: the higher the intensity, the better (i.e., less rough) is the surface. The

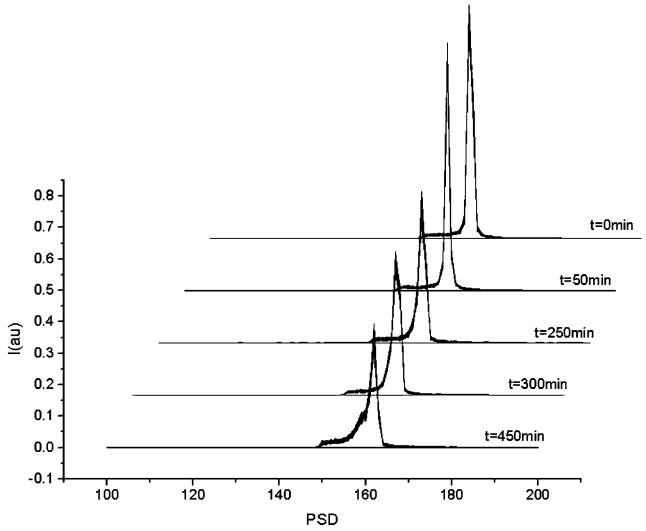

Figure 6. X-ray reflectivity peaks of sPI (EW = 792 g/equiv and X = 5) ionomer solution of 8 wt % at 50.9 °C for several drying times.

decrease of the intensity is interesting because one could have expected that it remains constant during the whole CRP. It may be explained by the ordering ionomer chains. Indeed, when the ionomer solution is poured onto the glass lamella, driving forces break the chains organization. As the drying time lasts several hours, the polymer chains may move and organize in order to minimize the interface energy and the interaction between ionomer chains. In the new environment, a new organization of the ionomer chains occurs. These observations are consistent with those of transport section. Furthermore,the present measurements show that, for a given thickness loss, by increasing

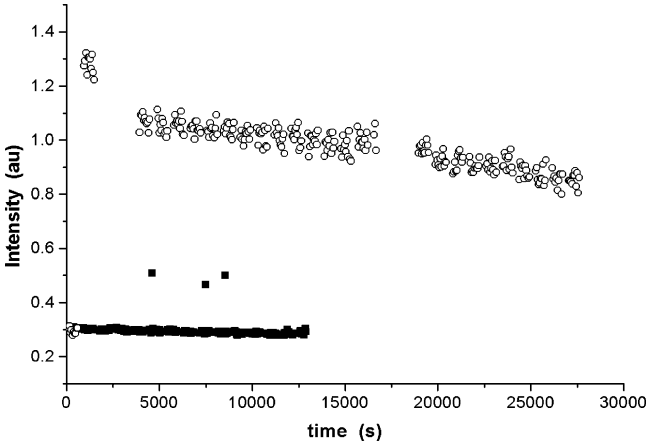

Figure 7. Variation of the intensity of X-ray reflectivity peaks of sPI (EW = 792 g/equiv and X = 5) ionomer solution of 8 wt % at 50.9 °C (open circle) and 42 °C (black square) vs drying time.

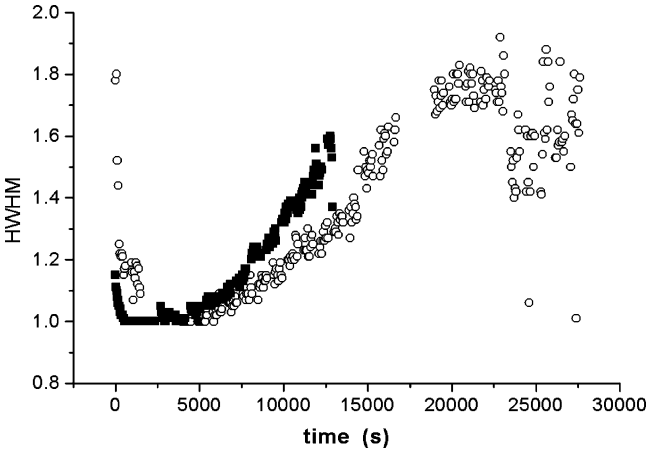

Figure 8. Variation of the HWHM of X-ray reflectivity peaks of sPI (EW = 792 g/equiv and X = 5) ionomer solution of 8 wt % at 50.9 °C (open circle) and 42 °C (black square) vs drying time.

the temperature, the surface quality is degraded more rapidly though we are still in CRP.

The variation of the HWHM vs time is plotted in Figure 8. HWHM is correlated with the structuration in the bulk sample. As for the intensity, the evolution is very slow in the course of time.

Despite the fact that evolutions of both intensity and HWHM are very slow, the properties of ionomer membrane are greatly affected by the casting process. Because of the very high viscosity of the ionomer solution and of the very weak diffusion of the ionomer chains, the initial constraint cannot be relaxed. One may propose to reduce the viscosity in order to reduce the casting influence. We have performed the experiences on a more dilute sample, but the results were the opposite of what was expected: the intensity was lost much more rapidly. The difference of solvation of the hydrophobic part and of the hydrophilic part of the sPI chains by *m*-cresol may induce such phenomena.

In Figure 3, the thickness loss of a sPI of smaller EW = 504 g/equiv but with the same block size (X = 5) is also plotted. The average slope is significantly higher (×2.5). The effect of the charge carried by the ionomer is thus an important parameter that drives the drying kinetic. In 1,4,5,8-naphthalene tetracarboxylic dianhydride and 4,4′-diamino-biphenyl 2,2′-disulfonic acid sPI, Genies et al.[7] have observed that the smaller the EW, the lower is the solubility of sPI in *m*-cresol. In addition, it has been shown that the structural organization of sPI membrane is all the more ordered since the EW is high.[14] The organization seems to be ruled by the hydrophobic part of the chains. The present results are consistent with these observations.

5. Conclusion

The casting of a charged polymer, a sPI ionomer, was studied. At first, the self-diffusion of $N(CH_3)_4^+$ ions inside two sPI membranes cast in a different manner, was compared: one was prepared by the usual protocol (hand coating) and a second by simple pouring. The diffusion is more anisotropic in the first membrane and it is attributed to shearing phenomena occurring during the hand-coating process. Besides, both membranes show several scales of structural organization. In addition, for the second kind of membrane we have observed that the surfaces during drying affect the transport properties. For a long enough drying time, the ionomer chains can move and organize and the more hydrophobic the surface, the slower is the ion diffusion through the complete membrane.

Second, we have studied the drying using X-ray reflectivity. The thickness loss of sPI ionomer solution in *m*-cresol was recorded in the course of time. In a first step, it decreases linearly with time and the process is ruled by the vapor pressure of *m*-cresol. The results indicate that the models developed for noncharged polymer drying processes may be suitable for ionomer. During this first period, the X-ray reflectivity signal can be recorded, but when approaching the end of this period, we observed a rapid loss of the X-ray reflectivity signal. This loss signs a degradation of the surface of the drying film (roughness). A correlation occurs between the drying process of the bulk sample and the structuration of the membrane surface. Moreover, we evidenced a strong influence of the quantity of charges carried by the ionomer chains: the higher the quantity, the faster is the drying kinetics.

Acknowledgment. We acknowledge the contribution of Nathalie Prulière and Jean-Pierre Simonin in the radiotracers experiments. We are deeply grateful to Armel Guillermo for his precious help on NMR experiments. The authors thank Laurent Rubatat for his help on conductivity measurements. We thank Ferdinand Volino and Bruno Alonso in offering stimulating discussions. The authors are indebted to the Centre Grenoblois de Résonance Magnétique (CGRM) for providing the NMR facilities and the Laboratoire Liquide Ionique et Interfaces Chargées (LI2C) for providing the radiotracers facilities. The authors are indebted to the CNRS/LMOPS and Régis Mercier for polymer synthesis and to the CEA-Le Ripault, Philippe Capron, and Franck Jousse for the membrane preparation. This work has been supported by the French Ministry of Research and Technology through the PREDIT and "Réseau technologique PACo" programs. ESRF awarded us the beamline SC985.

References and Notes

(1) Schlick, S. *Ionomers: Characterization, Theory and Applications*; CRC Press: Boca Raton, FL, 1996.

(2) Rollet, A.-L.; Diat, O.; Gebel, G. *J. Phys. Chem. B* **2002**, *106* (12), 3033−3036.

(3) Rubatat, L.; Rollet, A.-L.; Gebel, G.; Diat, O. *Macromolecules* **2002**, *35*, 4050−4055.

(4) Rollet, A.-L.; Gebel, G.; Simonin, J.-P.; Turq, P. *J. Polym. Sci. Polym. Phys. Ed.* **2001**, *39* (5), 548−558.

(5) Schmeller, A.; Ritter, H.; Ledjeff, K.; Nolte, R.; Thorwirth, R. EP 0,574,791 A2, 1993.

(6) Kerres, J.; Cui, W.; Reichle, S. J. *Polym. Sci., A* **1996**, *34*, 2421.

(7) Genies, C.; Mercier, R.; Sillion, B.; Cornet, N.; Gebel, G.; Pineri, M. *Polymer* **2001**, *42*, 359−373.

(8) Genies, C.; Mercier, R.; Sillion, B.; Petiaud, R.; Cornet, N.; Gebel, G.; Pineri, M. *Polymer* **2001**, *42*, 5097−5105.

(9) Yin, Y.; Fang, J.; Kita, H.; Okamoto, K.-i. *Chem. Lett.* **2003**, *32* (4), 328−329.
(10) Vallejo, E.; Pourcelly, G.; Gavach, C.; Mercier, R.; Pinéri, M. *J. Membr. Sci.* **1999**, *160*, 127−137.
(11) Cornet, N.; Diat, O.; Gebel, G.; Jousse, F.; Marsacq, D.; Mercier, R.; Pineri, M. *J. New Mater. Electrochem. Syst.* **2000**, *3*, 33−42.
(12) Piroux, F.; Espuche, E.; Mercier, R.; Pinéri, M.; Gebel, G. *J. Membr. Sci.* **2002**, *209*, 241−253.
(13) Blachot, J.-F.; Diat, O.; Putaux, J.-L.; Rollet, A.-L.; Rubatat, L.; Vallois, C.; Müller, M.; Gebel, G. *J. Membr. Sci.* **2003**, *214*, 31−42.
(14) Rollet, A.-L.; Diat, O.; Gebel, G. *J. Phys. Chem. B* **2004**, *108*, 1130−1136.
(15) Van de Witte, P.; Dijkstra, P. J.; van den Berg, J. W. A.; Feijen, J. *J. Membr. Sci.* **1996**, *117*, 1−31.
(16) Han, M.-J.; Bhattacharyya, D. *J. Membr. Sci.* **1995**, *98*, 191−200.
(17) Menut, P.; Pochat-Bohatier, C.; Deratani, A.; Dupuy, C.; Guilbert, S. *Desalination* **2002**, *145*, 11−16.
(18) Périé, M.; Périé, J. *Russ. J. Electrochem.* **1996**, *32* (2), 259−264.
(19) N. Cornet, PHD thesis, Université J. Fourier, 1999.
(20) Rollet, A.-L.; Simonin, J.-P.; Turq, P. *Phys. Chem. Chem. Phys.* **2000**, *2* (5), 1029.
(21) Wu, D.; Chen, A.; Johnson Jr., C. S. *J. Magn. Reson.* **1995**, *115*, 260−264.
(22) Cotts, R. M.; Hoch, M. J. R.; Sun, T.; Markert, J. T. *J. Magn. Reson.* **1989**, *83*, 252−266.
(23) Babinec, S. J.; Mussell, R. D.; Lundgard, R. L.; Cieslinski, R. *Adv. Mater.* **2000**, *12* (23), 1823−1833.
(24) Callaghan, P. T.; Coy, A.; Halpin, T. P. J.; MacGowan, D.; Packer, K. J.; Zelaya, F. O. *J. Phys. Chem.* **1992**, *97*, 7 (1), 651−662.
(25) Callaghan, P. T.; Stepisnik, J. Advances in magnetic and optical resonance; Academic Press: 1996; Vol. 19, p 325.
(26) Mitra, P. P.; Sen, P. N.; Schwartz, L. M.; Le Doussal, P. *Phys. Rev. Lett.* **1992**, *68* (24), 3555−3559.
(27) Coumans, W. J. *Chem. Eng. Process.* **2000**, *39*, 53−63.
(28) Stamm, M. *Adv. Polym. Sci.* **1992**, *100*, 357−400.